

Scientific paper

# Characterization of the Alkoxide-based Sol-gel Derived $\text{La}_{9.33}\text{Si}_6\text{O}_{26}$ Powder and Ceramic

Katarina Vojisavljević,<sup>1,\*</sup> Pierrick Chevreux,<sup>2</sup> Jenny Jouin<sup>3</sup>  
and Barbara Malič<sup>1</sup>

<sup>1</sup>Electronic Ceramics Department, Jožef Stefan Institute, Jamova 39, SI-1000 Ljubljana, Slovenia

<sup>2</sup>Ecole Nationale Supérieure de Céramique Industrielle E.N.S.C.I., Centre Européen de la Céramique, 12 Rue Atlantis, 87068 Limoges Cedex, France

<sup>3</sup>Science des Procédés Céramiques et Traitements de Surface (SPCTS), UMR 7315 CNRS, Université de Limoges, Centre Européen de la Céramique, 12 Rue Atlantis, 87068 Limoges Cedex, France

\* Corresponding author: E-mail: katarina.vojsavljevic@ijs.si  
Tel.: +386 1 477 3936; Fax: +386 1 477 3887

Received: 21-01-2014

*Dedicated to the memory of Prof. Dr. Marija Kosec.*

## Abstract

In this study, we report on the acid-catalysed synthesis of  $\text{La}_{9.33}\text{Si}_6\text{O}_{26}$  from lanthanum nitrate or acetate and silicon ethoxide (TEOS) in the ethanol solvent, upon the transition from liquid to amorphous and crystalline phases. The similarity of the Fourier transform infrared spectra of the lanthanum-salt solutions and lanthanum-silicon sols indicates that the lanthanum environment is not changed in the reaction of the La-salt with TEOS. In the nitric-acid catalysed synthesis, the hydrolysis reaction was almost instantaneous, as a consequence of a higher amount of water in this system, which contributed to a high level of chemical heterogeneity in the product. The acetic acid-based synthesis ensured a good mixing of the reagents at the nanometre level, which gave rise to the formation of the pure  $\text{La}_{9.33}\text{Si}_6\text{O}_{26}$  powder upon heating at 900 °C, and single phase ceramics with 94 % relative density after sintering at 1400 °C for 3 h in air, which is 200 °C lower temperature than usually reported for the apatite material.

**Keywords:**  $\text{La}_{9.33}\text{Si}_6\text{O}_{26}$  apatite; sol-gel process; FTIR; X-ray diffraction; fuel cells

## 1. Introduction

Recently, much attention has been paid to production of the solid ionic conductors, especially those that found the applicability in solid oxide fuel cell (SOFC) systems as electrolyte materials. The operating properties of the fuel cell, their efficiency and life-time are strongly connected with a quality of the electrolyte material and can be tuned and improved by a proper selection of the electrolyte, which has to possess sufficiently large oxygen ion conductivity at the operating temperature and good thermal expansion matching with the electrode materials.

Over the past decade research on electrolyte material has been mainly focused on a new class of materials with the apatite  $\text{Ln}_{10-x}(\text{MO}_4)_6\text{O}_{2+y}$  structure (Ln is a metal

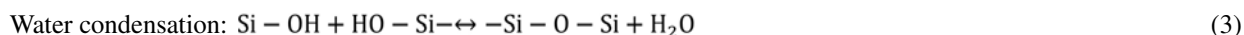
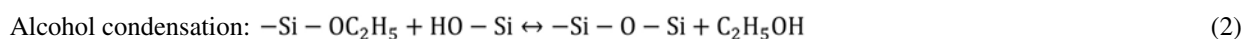
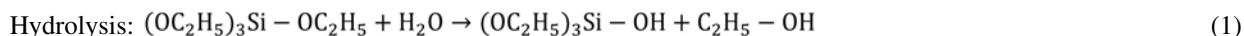
such as rare-earth or alkaline earth, M is a p-block element such as Si, Ge, or Al).<sup>1-3</sup> The main idea is to replace the yttria stabilized zirconia (YSZ),<sup>4,5</sup> the electrolyte usually utilized in the fuel cells that have shown the maximum performances at a high operating temperatures (800 °C–1100 °C) with apatites, which possess high oxygen ionic conductivity at intermediate temperatures and low activation energy ( $4 \times 10^{-3}$  S/cm at 500 °C and 0.6–0.8 eV,<sup>6</sup>). Decreasing the operating temperature to the intermediate temperatures, a problem with the thermal instability of the solid electrolyte could be avoided and the lifetime of the fuel cell prolonged.

Among all apatites, lanthanum silicate,  $\text{La}_{9.33}\text{Si}_6\text{O}_{26}$  is the most promising candidate to fulfill the demands for technical application. The  $\text{La}_{9.33}\text{Si}_6\text{O}_{26}$  has been usually

prepared by conventional solid state synthesis route,<sup>3,7–11</sup> where high temperatures (1600 °C–1800 °C),<sup>9</sup> with intermediate wet-milling steps are needed to achieve the single phase material, and long sintering cycles at elevated temperatures are required to densify them,<sup>10,11</sup>. However, secondary phases, such as LaSi<sub>2</sub>O<sub>5</sub> and La<sub>2</sub>Si<sub>2</sub>O<sub>7</sub>,<sup>8</sup> could remain in the system and deteriorate the conductivity of the ceramic electrolyte.

The alkoxide based sol-gel processing of the La<sub>9,33</sub>Si<sub>6</sub>O<sub>26</sub> ceramic powders has been proven as a better method from the aspect of homogeneity and purity than the solid state synthesis.<sup>12,13</sup> By choosing the proper conditions, the reactants in the sol-gel synthesis could have a high reactivity and mobility, and react easily and completely, which can greatly reduce the synthesis temperature of the apatite-type La<sub>9,33</sub>Si<sub>6</sub>O<sub>26</sub> powders. Due to the lower temperature employed in the synthesis, the powder with a better homogeneity and particle size distribution can be obtained, and that could be a crucial factor in reducing the sintering temperature below 1600 °C required for the dense and single phase ceramics by conventional solid state synthesis route.

In this paper, the La<sub>9,33</sub>Si<sub>6</sub>O<sub>26</sub> gels were prepared through a simple addition of silicon ethoxide, TEOS to a solution of La(III) salts with acetic acid or nitric acid as the catalyst in ethanol. TEOS reacts with the crystal water from the salts, i.e., it undergoes the hydrolysis reaction (Eq. (1)). The condensation reaction may occur before all the hydroxo groups have been generated (Eq. (2), (3)).



The ethanol forms as a by-product of the hydrolysis reaction and it can play an important role in the formation of the homogeneous gel, since TEOS is not miscible with water. According to Célérier and co-workers,<sup>12</sup> the H<sub>2</sub>O/Si molar ratio and TEOS concentration may influence both the hydrolysis and condensation rates, and further the homogeneity of the gel. The lower H<sub>2</sub>O/Si molar ratio, the smaller amount of impurities (La<sub>2</sub>O<sub>3</sub>, La<sub>2</sub>SiO<sub>5</sub>, La<sub>2</sub>Si<sub>2</sub>O<sub>7</sub>) incorporated into the apatite structure. The minimum value of the water present in the sols is related to the crystallization water of lanthanum salts. The hydrolysis of the siloxane bonds can be promoted at the higher H<sub>2</sub>O/Si ratio, leading to the inadequate homogeneity in the polymer network. Also, it was concluded by Célérier and co-workers,<sup>12</sup> that a higher TEOS concentration is important for the phase-purity of the powder obtained upon heating the gel in air at 1000 °C. It was also found that there is no influence of the volumetric ratio of the catalyst to TEOS on the nature of phases, if it is lower than 8.

Within this work, the sols were prepared taking into account the optimum reaction conditions proposed by Célérier and co-workers,<sup>12</sup> meaning that the hydrolysis molar ratio was kept as low as possible, while the TEOS concentration was high. To understand the process of gelation more completely, the different steps, which resulted in the formation of the sols and gels, i.e. the La-nitrate/acetate-alkoxide synthesis pathways were analysed for the first time by FTIR. Phase compositions of the xerogels and powders were also investigated by XRD and FTIR analyses. In addition, the pure La<sub>9,33</sub>Si<sub>6</sub>O<sub>26</sub> powder was used for the synthesis of the single phase ceramics.

## 2. Materials and Methods

Lanthanum nitrate x-hydrate, La(NO<sub>3</sub>)<sub>3</sub> · xH<sub>2</sub>O, denoted LN, (99.9%, Sigma-Aldrich, Taufkirchen, Germany), lanthanum acetate y-hydrate, La(CH<sub>3</sub>COO)<sub>3</sub> · yH<sub>2</sub>O, denoted LA, (99.99%, Alfa Aesar, Karlsruhe, Germany), and silicon ethoxide or TEOS, Si(OC<sub>2</sub>H<sub>5</sub>)<sub>4</sub> (99.8%, Alfa Aesar, Karlsruhe, Germany) were used as reagents. The absolute alcohol (Carlo Erba SAS, Val De Reuil, France) was used as the solvent, along with the acetic acid (100%, Applichem, Darmstadt, Germany) or nitric acid (65% (14.4 M), Applichem, Darmstadt, Germany) as the catalysts.

Knowing the hygroscopic nature of lanthanum nitrate and lanthanum acetate, and in order to keep the stoichiometric relationship between La/Si metal ions, special

attention was paid to the amount of water present in both salts. The thermal decomposition of the La-reagents was studied by thermogravimetric and differential thermal analysis (TG/DTA, NETZSCH STA 409) in flowing air atmosphere with the heating rate of 10 °C/min. The TG-DTA curves are shown in Fig. 1. The TG-DTA curves display the typical decomposition pathways of these compounds, see<sup>14–17</sup>. The total weight loss observed upon heating the lanthanum nitrate from room temperature to 800 °C is 63.32% (see Fig. 1a), which is 0.9% higher than the theoretical value. The dehydration of the salt can be correlated with the weight loss of 25.84% in TG curve, and it is followed by endotherms at 172 °C and 205 °C in the DTA curve. The calculated molar weight of the lanthanum nitrate salt is 438.45 g/mol, thus the compound can be described as La(NO<sub>3</sub>)<sub>3</sub> · 6.3H<sub>2</sub>O.

The total weight loss observed upon heating the La(CH<sub>3</sub>COO)<sub>3</sub> · yH<sub>2</sub>O to 1000 °C in air is 53.33 % (see Fig. 1b), which is 0.8 % higher than the theoretical value.

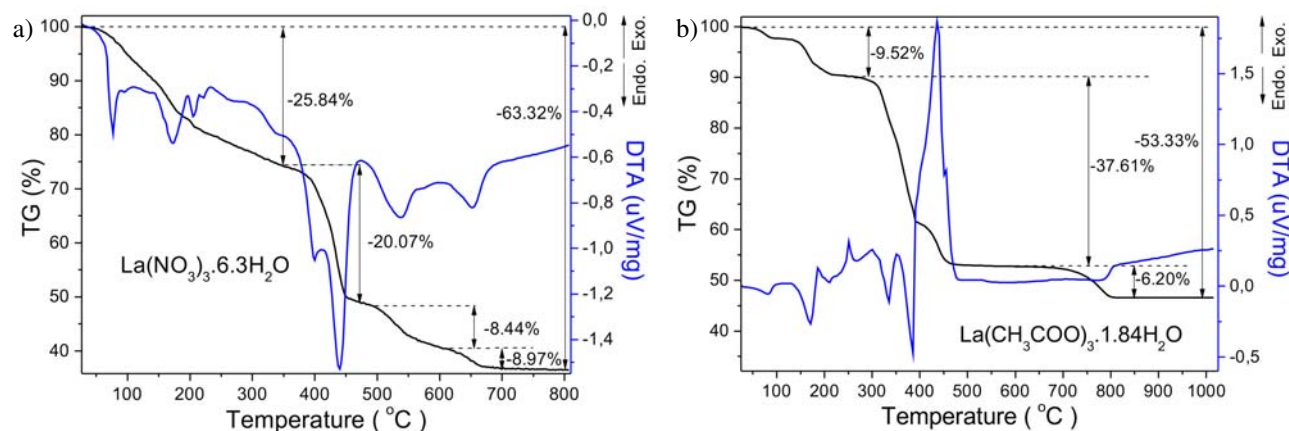


Figure 1. TG-DTA curves of a)  $\text{La}(\text{NO}_3)_3 \cdot 6.3\text{H}_2\text{O}$  and b)  $\text{La}(\text{CH}_3\text{COO})_3 \cdot 1.84\text{H}_2\text{O}$  reagents. (Colour online)

The first two losses in weight, registered in the range from room temperature to 220 °C, and coupled with two endothermic events at 170 °C and 210 °C, could be assigned to the evaporation of the physisorbed and chemisorbed water, respectively. The weight loss related to the water evaporation is 9.52 %, so the molar weight of the lanthanum acetate hydrate is 349.19 g/mol and the formula of the salt is  $\text{La}(\text{CH}_3\text{COO})_3 \cdot 1.84\text{H}_2\text{O}$ .

All steps involved in preparation of the apatite-type  $\text{La}_{9.33}\text{Si}_6\text{O}_{26}$  are presented schematically in Fig. 2 and explained in details below. A clear solution was prepared by dissolving  $\text{La}(\text{NO}_3)_3 \cdot 6.3\text{H}_2\text{O}$  in a mixture of absolute ethanol and acetic acid (La-nitrate route), or  $\text{La}(\text{CH}_3\text{COO})_3 \cdot 1.84\text{H}_2\text{O}$  in a mixture of absolute ethanol and nitric acid

(La-acetate route). Then, TEOS was added to the solution, taking into account the stoichiometric relationship between the metal ions,  $\text{La}/\text{Si} = 9.33/6$ . To be more precise, the parameters for the preparation of the sol, presented in the La-nitrate route were:  $\text{H}_2\text{O}/\text{Si} = 9.6$ , concentration of Si,  $c_{\text{Si}} = 0.9 \text{ mol/dm}^3$  and acetic acid/TEOS volumetric ratio = 2, while for the La-acetate route they were the next:  $\text{H}_2\text{O}/\text{Si} = 2.9$ ,  $c_{\text{Si}} = 0.5 \text{ mol/dm}^3$  and nitric acid/TEOS volumetric ratio = 2. The solution was agitated for 1 h, and then transferred to the oil bath, where it was continuously stirred at the temperatures between 60 °C to 70 °C for 82 min in the case of the La-nitrate route and 40 min for the La-acetate route. The rate of the gel formation was higher in the case of the La-acetate route. The viscous white-

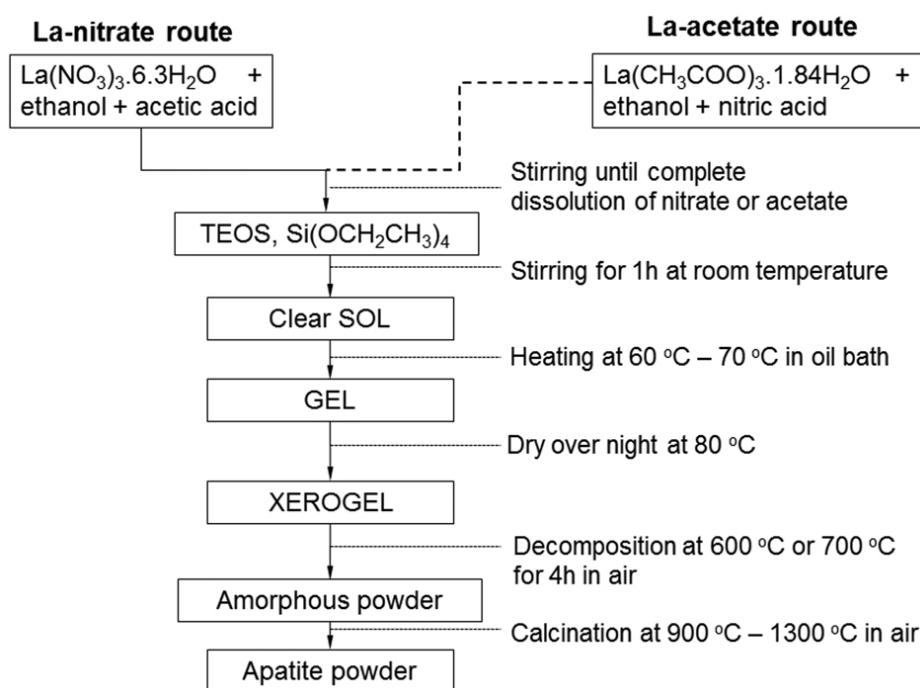


Figure 2. The flow chart of the process used for the preparation of the  $\text{La}_{9.33}\text{Si}_6\text{O}_{26}$  powder.

translucent gel was heated in a drying oven at 80 °C over the night. The formation of the xerogel occurred within several hours of heating. The thermal behaviour of xerogels by using thermogravimetric and differential thermal analysis (TG/DTA, NETZSCH STA 409) coupled with a mass spectrometer (Thermostat GSD300T Balzers) for the evolved gas analysis (EGA-MS). The experiments were done in flowing air atmosphere with the heating rate of 2 °C/min.

The xerogels were heat-treated at 700 °C (La-nitrate route) or 600 °C (La-acetate route) in a muffle furnace and subsequently wet milled for 1 h in a planetary mill (Retsch PM400, Retsch GmbH, Haan, Germany, zirconia vials and balls) in isopropyl alcohol (IPA), then dried at 70 °C, uniaxially pressed at the pressure of 50 MPa into the pellets of 6 mm in diameter and calcined at 900 °C (for 10 h), 1000 °C (for 3 h) and 1300 °C (for 3 h).

Ethanol solutions of the LN and LA in the presence of the selected catalyst are denoted LN-sol and LA-sol, respectively. Ln-Si reaction products after different stages of processing are denoted as LNS or LAS -sol, -gel and -xero, and after heating at 700 °C or 600 °C as LNS\_700 and LAS\_600, respectively.

To prepare the single phase ceramic sample, the powders calcined at 900 °C were milled in IPA for 30 min in a planetary mill to break up the agglomerates and to reduce the diffusion paths. Those powders are marked as LNS\_900 and LAS\_900. The milled powders were submitted to the calcination at 1300 °C and 1500 °C to check the phase purity. After this experiment, the LNS\_900 powder was chosen for the ceramic processing. The powder was uniaxially pressed into pellets of 8 mm in diameter at 100 MPa and subsequently by cold isostatic pressing at 400 MPa, and sintered in air at 1400 °C for 3 h, with heating and cooling rates of 5 °C/min and 2 °C/min.

The morphology of the powders was examined by the field emission scanning electron microscope FE-SEM (JEOL JSM 7600F, Tokyo, Japan). The powder was ultrasonically dispersed in IPA and the suspension was spread on the surface of the sample holder. After alcohol evaporation a 5 nm thick layer of carbon was deposited on the powder surface under the vacuum and analysed. The microstructure of the sintered sample was analysed using the scanning electron microscope, SEM (JEOL JSM 5800, Tokyo, Japan). For the analysis, the sample was cut, the cross-section was polished and then thermally etched at 1350 °C for 10 min.

The particle sizes, expressed as the median value ( $d_{50}$ ), and size distributions (PSD) of the powders were determined from the area distributions measured by a laser granulometer (Microtrac S3500 Particle Size Analyzer, Montgomeryville, PA).

The phase composition of the powders was analysed by PANalytical diffractometer (X'Pert PRO MPD, Almelo, Netherlands, Bragg-Brentano geometry using the  $\text{Cu-K}\alpha$  radiation and X'Celerator detector configured in ref-

lection geometry). The data acquisition was done in the step scan mode ( $2\theta = 0.034^\circ$ , integration time 100 s) in the angular range  $2\theta = 10\text{--}70^\circ$ . The phases were identified with the X'Pert High Score package, using the PDF-2 reference patterns database. The crystallite size of the  $\text{La}_{0.33}\text{Si}_6\text{O}_{26}$  powder was calculated using the Debye-Scherrer equation (Eq. (4)):

$$L = \frac{k\lambda}{\beta(2\theta)\cos\theta} \quad (4)$$

where  $L$  is the crystallite size,  $\lambda$  the wavelength ( $\text{Cu}_{K\alpha 1}$ , 0.15406 nm),  $k$  the dimensionless shape factor ( $= 0.94$ ),  $\theta$  the Bragg angle. The half-width of the diffraction line  $\beta(2\theta)$  in radians was taken as the experimental half-width ( $\beta_{\text{exp}}$ ) and was corrected for experimental broadening ( $\beta_{\text{ins}}$ ) according to:

$$\beta(2\theta) = (\beta_{\text{exp}}^2 - \beta_{\text{ins}}^2)^{1/2} \quad (5)$$

The  $\beta_{\text{ins}}$  was measured experimentally by a highly crystalline  $\text{LaB}_6$  powder.

Fourier Transform Infrared (FTIR) spectra were recorded by a Perkin Elmer Spectrum 100 spectrometer in the attenuated total reflectance (ATR) mode. The resolution was set at 4  $\text{cm}^{-1}$  in the spectral range covering 4000–400  $\text{cm}^{-1}$ .

The density was calculated from the mass and dimensions and also confirmed by the Archimedes principle. The relative density was calculated using the theoretical value of  $\rho_{\text{th}} = 5.318 \text{ g}\cdot\text{cm}^{-3}$ , extracted from the cell parameters.

## 3. Results and Discussion

### 3.1. Characterization of the Sols and Gels

Individual steps of the sol-gel synthesis of lanthanum silicate, starting by dissolving the La-salt in ethanol in the presence of a catalyst with TEOS, and the reaction products were analysed by FTIR spectroscopy (Fig. 3).

The spectrum of the solvent with the acetic acid as the catalyst, presented in Fig. 3a shows the broad O-H band in the region 3650  $\text{cm}^{-1}$ –2300  $\text{cm}^{-1}$ , superimposed onto the sharp C-H stretching bands of the ethanol (2979  $\text{cm}^{-1}$ , 2938  $\text{cm}^{-1}$  and 2902  $\text{cm}^{-1}$ ) and acetic acid (3027  $\text{cm}^{-1}$ , 2929  $\text{cm}^{-1}$ , 2686  $\text{cm}^{-1}$ , 2628  $\text{cm}^{-1}$ , 2555  $\text{cm}^{-1}$ ). The sharp mode at 1707  $\text{cm}^{-1}$  with a neck at the higher frequency (1756  $\text{cm}^{-1}$ ) is due to the C=O stretching vibration of the carboxyl group. The next band at 1400  $\text{cm}^{-1}$  could be attributed to the O-H stretch, modified by the C-H bending bands from both acetic acid and ethanol. The bands at 1285  $\text{cm}^{-1}$  and 1239  $\text{cm}^{-1}$ , typical for the C-O stretching vibration of the carboxyl group, are slightly changed by -CH<sub>3</sub> bending bands from both acetic acid and ethanol. The characteristic C-O stretching vibrations from the ethanol

are positioned at  $1085\text{ cm}^{-1}$  to  $1046\text{ cm}^{-1}$ . The broad band between  $983\text{ cm}^{-1}$  and  $696\text{ cm}^{-1}$  includes the O-H vibration combined with bands from acetic acid and ethanol. The bands at  $607\text{ cm}^{-1}$  and  $479\text{ cm}^{-1}$  are typical for the acetic acid.

A broad band observed in the range of  $3600\text{--}3100\text{ cm}^{-1}$  in the spectrum of lanthanum nitrate, LN, (see Fig. 3a) is attributed to the O-H stretching vibrations. The sharp bands in the range  $1650\text{--}700\text{ cm}^{-1}$  could be mainly related to the vibrations of the nitrate group.<sup>14, 18</sup> Additionally, the spectrum presents the band at  $1637\text{ cm}^{-1}$ , which could be assigned to the bending mode of the lattice coordinated water.

The spectrum of the LN-sol contains the characteristic bands of both LN and the solvent with the acetic acid. Especially, the presence of the strong bands at  $817\text{ cm}^{-1}$  and  $736\text{ cm}^{-1}$ , typical for the nitrate group and the shift of the strong band, related to OH and CH vibrations modified with  $\text{NO}_3^-$  vibrations, from  $1400\text{ cm}^{-1}$  to  $1440\text{ cm}^{-1}$  indicates that the nitrate ions remained strongly coordinated to the La ions.

In the next step, the LNS-sol was synthesized by the reaction of the LN-sol with TEOS. The FTIR spectra of the LNS-sol and LN-sol are similar, indicating that the lanthanum environments in both sols are not influenced by the addition of TEOS. The situation stays unchanged even after the gelation.

In Fig. 3b the course of the acetic-acid catalyzed synthesis is depicted. The spectrum of ethanol with the nitric acid, as a catalyst, S+NA, possesses the wide band

$3716\text{ cm}^{-1}\text{--}3035\text{ cm}^{-1}$ , typical for the O-H stretching vibration, followed by the modes at  $2979\text{ cm}^{-1}$ ,  $2938\text{ cm}^{-1}$  and  $2902\text{ cm}^{-1}$ , due to C-H stretching vibrations in ethanol. The band at  $1658\text{ cm}^{-1}$  is due to  $\text{NO}_2$  asymmetric stretching vibration from the nitric acid, while the broad band centered at the  $1418\text{ cm}^{-1}$  could be explained as the combination of the strong and sharp NOH bending vibration from the nitric acid and medium and sharp  $-\text{CH}_2$ , observed in FTIR spectrum of ethanol (the spectrum was not shown here) at  $1454\text{ cm}^{-1}$ ,  $1418\text{ cm}^{-1}$ . The band at  $1287\text{ cm}^{-1}$  is due to  $\text{NO}_2$  symmetric stretching, mixed with the NOH bending, as well as with the  $-\text{CH}_3$  bending vibrations. The characteristic C-O stretching vibrations from the ethanol are in the range from  $1117\text{ cm}^{-1}$  to  $982\text{ cm}^{-1}$ , while the  $\text{NO}'$  stretching vibration, where with the O' is labeled the oxygen atom to which the hydrogen atom is attached, is occurred at  $944\text{ cm}^{-1}$ . The modes at  $688\text{ cm}^{-1}$  and  $639\text{ cm}^{-1}$  correspond to the combined  $\text{ONO} + \text{ONO}'$  and  $\text{ONO}'$  bending vibrations from the nitric acid.

The broad band that appears in the spectrum of Lactate, LA, in the region  $3600\text{--}2900\text{ cm}^{-1}$  is assigned to the -OH vibration from the water, combined with the asymmetric/symmetric vibrations of the C-H group from the  $\text{CH}_3\text{COO}^-$ , positioned at  $3012\text{ cm}^{-1}$  and  $2929\text{ cm}^{-1}$ . The characteristic bands observed at  $1551\text{ cm}^{-1}$ ,  $1449\text{ cm}^{-1}$ ,  $668\text{ cm}^{-1}$  and  $613\text{ cm}^{-1}$  are due to asymmetric/symmetric stretching, deformation and rocking vibrations of the  $\text{COO}^-$  group, respectively. Asymmetric/symmetric stretching and rocking vibrations of the  $\text{CH}_3$  group from the  $\text{CH}_3\text{COO}^-$  appear in the spectrum at the positions of  $1392$

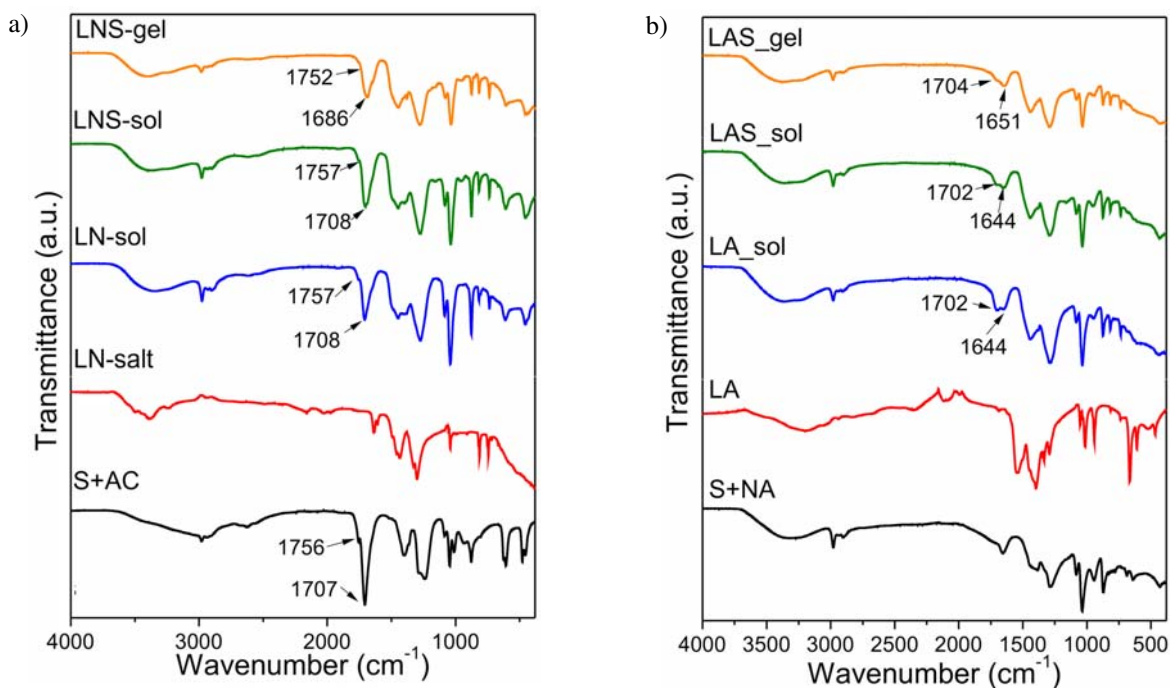


**Figure 3.** FTIR spectra of the solvent + acetic acid (S+AC), LN, LN-sol, LNS-sol and LNS-gel a) and the solvent + nitric acid (S+NA), LA, LA-sol, LAS-sol and LAS-gel b). (Colour online)

$\text{cm}^{-1}$ ,  $1333 \text{ cm}^{-1}$  and  $1053/1013 \text{ cm}^{-1}$ , while the band at  $942 \text{ cm}^{-1}$  could be explained by C-C stretching motions.<sup>16</sup>

The spectrum of the LA-sol contains characteristic bands of both  $\text{La}(\text{CH}_3\text{COO})_3 \cdot 1.84\text{H}_2\text{O}$  and solvent with  $\text{HNO}_3$  catalyst.

In the next step, the LAS-sol was synthesized by the reaction of the LA-sol with TEOS. There is no significant change in the FTIR spectrum of the LAS-sol as compared to the LA-sol, indicating that the lanthanum environments in both sols are similar and not influenced by the addition of TEOS.

The spectrum of the LAS-gel shows the presence of the same bands like the LAS-sol. A slightly lower intensity of the bands could be explained by a partial evaporation of water during this stage of synthesis.

The FTIR results suggest that no La-Si correlations are established during the hydrolysis/condensation and thermolysis steps of the proposed sol-gel synthesis. It seems that the lanthanum cations are more or less homogeneously distributed along the -Si-O-Si- chains in the gel network.

In Fig. 4, the FTIR spectra of the LNS-sol and LAS-sol were additionally compared with the aim to establish the difference in lanthanum environments and to follow the presence of water in both sols. The strong bands approximately at  $1440 \text{ cm}^{-1}$ ,  $817 \text{ cm}^{-1}$  and  $736 \text{ cm}^{-1}$ , which are also observed in the spectrum of the lanthanum nitrate, indicate that the nitrate ions are strongly coordinated to the La ions in both sols. Comparing the intensities of the modes at  $3250 \text{ cm}^{-1}$ ,  $1440 \text{ cm}^{-1}$ ,  $945 \text{ cm}^{-1}$ , which are mainly correlated to the O-H vibrations from the water, it becomes obvious that the amount of water is higher in the LAS-sol than in the LNS-sol, even if this value was 3x higher in the lanthanum nitrate than in the lanthanum acetate according to TG-DTA. The additional water comes from the nitric acid, which forms an azeotrope mixture with water. The nitric acid is also a catalyst for the hydrolysis reaction and furthermore, it is a stronger acid than the acetic acid. Thus the hydrolysis reaction is favoured, process of gelation is almost instantaneous in LAS-sol, as confirmed by the experiment and could be a reason for possible poor homogeneity of the LAS-gel network.<sup>12,19,20</sup>

Furthermore, the sharp mode at  $1707 \text{ cm}^{-1}$  with a neck at the higher frequency ( $1756 \text{ cm}^{-1}$ ) associated to the C=O asymmetric and symmetric stretching vibration from the carboxyl group in S+AC (see Fig. 3a) are slightly shifted from this positions to the higher wavenumber values ( $1757 \text{ cm}^{-1}$  and  $1708 \text{ cm}^{-1}$ ) in the FTIR spectrum of the LN-sol and LNS-sol, and to the lower values ( $1702 \text{ cm}^{-1}$  and  $1644 \text{ cm}^{-1}$ ) in the FTIR spectrum of the LA-sol and LAS-sol (see Fig. 3 and Fig. 4). It is known that its position varies slightly depending on what sort of compound it is in.<sup>21</sup> The additional shifting of the C=O asymmetric and symmetric vibration is observed after gelation, i.e. their positions in the LNS-gel are  $1752 \text{ cm}^{-1}$  (weak) and  $1686 \text{ cm}^{-1}$  (strong) and in the LAS-gel at  $1704 \text{ cm}^{-1}$  (strong) to

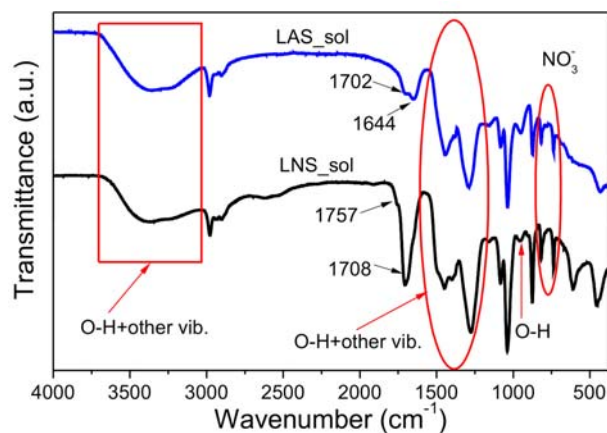


Figure 4. FTIR spectra of the LNS-sol and LAS-sol. (Colour online)

$1651 \text{ cm}^{-1}$  (strong) (see Fig. 3). According to these results, the acetic acid does not participate in ligand formation in LN-sol and LNS-sol, while the strong C=O band at  $1686 \text{ cm}^{-1}$  in LNS-gel indicates the weak interaction between acetic acid and OH groups from the La-ligand or even the interaction between two acetic acid molecules. In contrast to LN-sol and LNS-sol, the shifting of the asymmetric and symmetric C=O bands to the lower values ( $1702 \text{ cm}^{-1}$  and  $1644 \text{ cm}^{-1}$ ) in LA-sol and LAS-sol, as well as in LAS-gel, and the difference of  $58 \text{ cm}^{-1}$  between them reveals that the acetate groups are bonded by a chelating bidentate configuration and participate in the La-ligand formation.<sup>21,22</sup>

### 3. 2. Thermal Decomposition of Xerogels

The TG-DTA curves of both LNS-xero and LAS-xero, are shown in Fig. 5. The thermal decomposition of the LNT-xero upon heating to  $1000 \text{ }^\circ\text{C}$ , according to TG curve shown in Fig. 5a, undergoes in three steps and the total weight loss observed in this temperature range is 51.82%. The first weight loss of 16.58%, occurred in the range from room temperature to  $254 \text{ }^\circ\text{C}$  corresponds to dehydration-residual solvent evaporation and it can be separated into two distinct steps: the first one, from room temperature to  $150 \text{ }^\circ\text{C}$ , which can be attributed to removal of the physisorbed water and water from solvent, and the second one, from  $150 \text{ }^\circ\text{C}$  to  $254 \text{ }^\circ\text{C}$ , indicative for the removal of carbon dioxide and water. The same was confirmed by EGA analysis, where the evolution of the  $\text{H}_2\text{O}$  (mass fragment 18) and  $\text{CO}_2$  (mass fragment 44) gaseous species were detected in the temperature range from RT to  $254 \text{ }^\circ\text{C}$ . Furthermore, the evolution of the  $\text{NO}_2$  (mass fragment 46) in a small extent was observed at  $220 \text{ }^\circ\text{C}$ . The second step ( $254 \text{ }^\circ\text{C}$ – $390 \text{ }^\circ\text{C}$ ) with the weight loss of 20.97%, coupled with an exothermic event at  $323 \text{ }^\circ\text{C}$ , is attributed to decomposition of the organic (acetate and alkoxide) and nitrate groups, and it is accompanied by the evolution of  $\text{H}_2\text{O}$ ,  $\text{CO}_2$ ,  $\text{NO}_2$  and traces of acetone

(mass fragment 58) with maxima at approximately 320 °C in EGA curve. The presence of a low amount of acetone in the EGA is due to a stepwise decomposition pathway as in La-acetate alone.<sup>16,23</sup> The third step registered in the temperature range from 390 °C to 950 °C, with the weight loss of 14.26%, could be related to the removal of the carbonates and oxidation of the carbon residues. Processes of decarboxylation are exothermic and the crystallization of the lanthanum silicate phase occurs at the same temperature interval. The main volatile species in is the CO<sub>2</sub> with the maxima at 536 °C and 835 °C in EGA curve.

According to the TG curve shown in Fig. 5b, the thermal decomposition of the LAS-xerogel upon heating to 1000 °C undergoes in two steps and the total weight loss observed in this temperature range is 54.64 %. The first weight loss of 20.37 % between room temperature and 200 °C is due to evaporation of water, residual solvent and organics, and it is coupled with the strong exothermic peak at 156 °C. According to EGA, a small amount of physisorbed water evaporates at 102 °C, while the maximum of water evaporation is occurred at 153 °C along with the maxima of the CO<sub>2</sub>, NO<sub>2</sub> and acetone evaporation at the same temperature, confirming the decomposition of organics (alkoxide, acetate) and nitrates. A weight loss of 33.69 % is related to further elimination of organics and water and it is accompanied with two exo-DTA peaks at 220 °C and 363 °C. At both temperatures the main volatile species are CO<sub>2</sub>, H<sub>2</sub>O and NO<sub>2</sub>. The

exothermic peak at approximately 865 °C, which has no associated weight loss, is due to the crystallization of the LSO powder.

The different decomposition pathways of the LNS\_xero and LAS\_xero indicate the different bonding of the water and organic species during the gel formation, which is also confirmed by FTIR analysis.

In order to analyze the composition of the xerogels, the FTIR spectra of the LNS-xero and LAS-xero were collected, see Fig. 6. Obviously, the most of the water and alcohol evaporated during the drying step at 80 °C. The bands at 1440 cm<sup>-1</sup>, 1318 cm<sup>-1</sup>, 1277 cm<sup>-1</sup>, 1029 cm<sup>-1</sup>, 807 cm<sup>-1</sup>, and 741 cm<sup>-1</sup> are assigned to the nitrates and re-

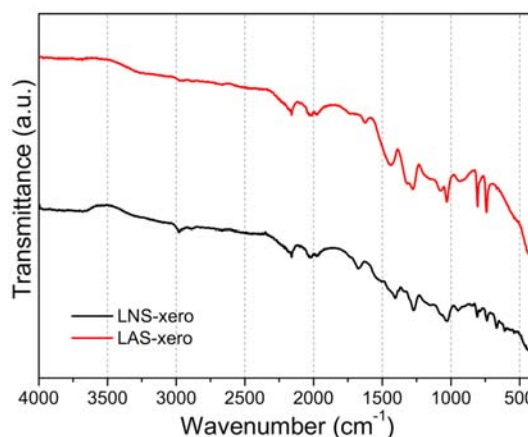


Figure 6. FTIR spectra of the LNS-xero (black curve) and LAS-xero (red curve). (Colour online)

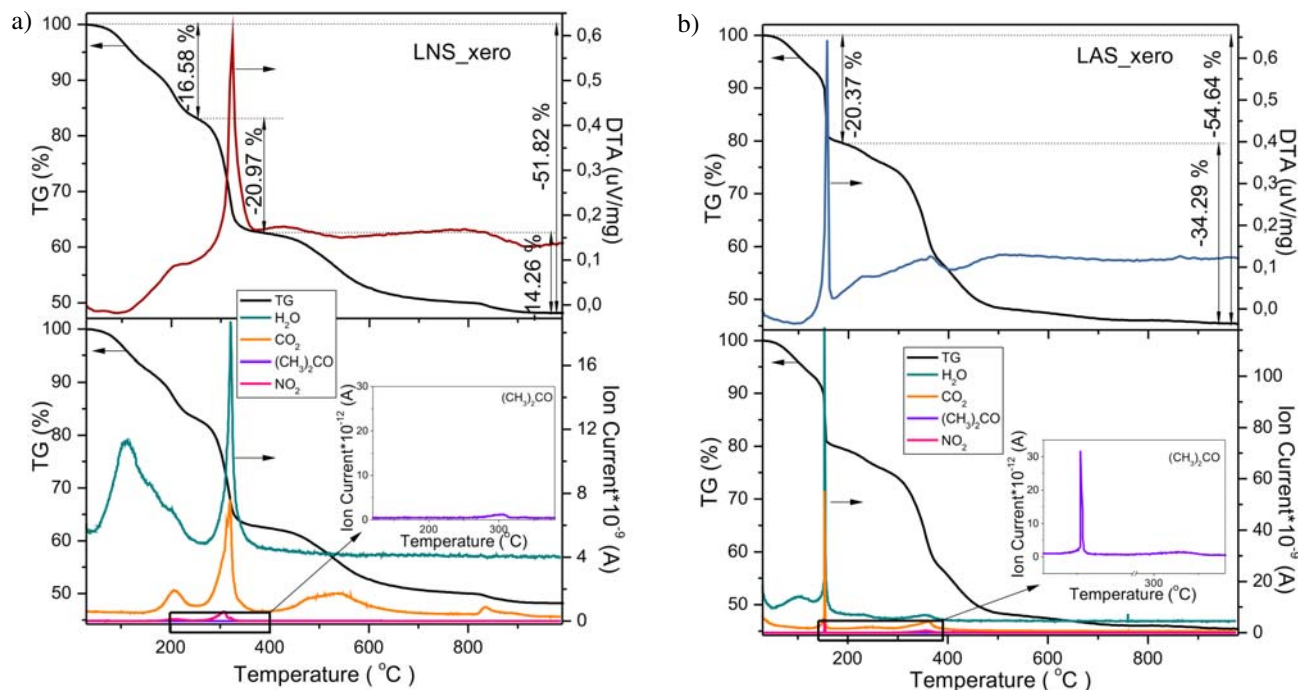


Figure 5. Simultaneous TG-DTA-EGA-MS analysis of LNS\_xero a) and LAS\_xero b). Insets show the amount of acetone released during the heating of xerogels. (Colour online)

sidual functional groups present in the xerogels (from acetates). There is no indication that the link between La and Si species was established.

Having in view the DTA and FTIR data of both xerogels and the fact that the xerogels still possess organic residues, it becomes obvious that the reactions upon heating to 400 °C could be highly exothermic. So, the calcination temperatures were settled at 240 °C, 320 °C, 420 °C, to avoid any kind of violent reaction upon heating in the furnace, and then to 700 °C (LNS-xero) or 600 °C (LAS-xero), to obtain the amorphous lanthanum silicate powders without any residues and polycrystalline oxide phase. A slow heating rate of 1 °C/min was used, followed with a dwell-time of 1 h for the first three steps, and 4 h for the final step. As there was no significant weight loss above 900 °C in both TG curves, and the exothermic peak was observed at approximately 900 °C for both LNS-xero and LAS-xero by DTA, it was reasonable to expect that the pure lanthanum silicate would crystallize upon heating to this temperature.

### 3. 3. Crystallization of Xerogels

Since no reaction between La and Si species could be determined by FTIR analysis of the sols, gels and xerogels, the reaction between intimately mixed lanthanum and silicon species could take place only upon heating. The phase composition of the LNS-xero and LAS-xero, before and after calcination at various temperatures in air was analyzed by XRD and the patterns are displayed in Fig. 7.

The XRD pattern of the LNS\_xero reveals its amorphous nature. A broad peak at around 29° witnessing the amorphous nature of the powder even after heating to 700 °C (see Fig. 7a). After heating at 900 °C, the precursor powder crystallizes in the pure apatite  $\text{La}_{9.33}\text{Si}_6\text{O}_{26}$  phase (PDF 00-049-0443, P63/m), which is stable upon heating to 1000 °C. Calcination at higher temperatures resulted in the formation of lanthanum-rich phases. Monoclinic  $\text{La}_2\text{SiO}_5$  (PDF 00-040-0234, P21/c) and tetragonal  $\text{La}_2\text{Si}_2\text{O}_7$  (PDF 01-072-2456, P41) were found in the powder calcined at 1300 °C. A study of Fukada and co-wor-

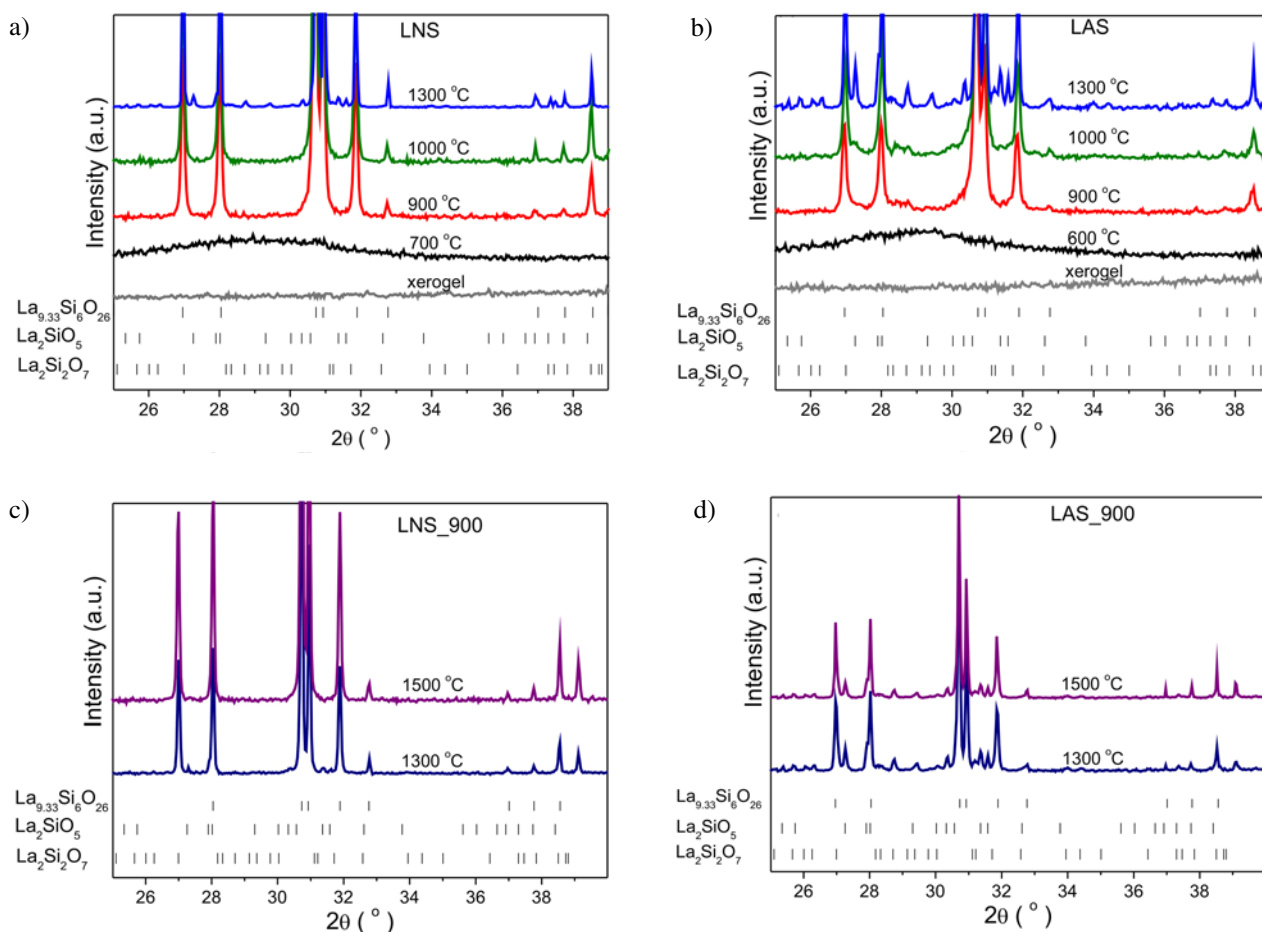


**Figure 7.** XRD patterns of the a) LNS\_xero and powders obtained by calcination of the LNS\_xero at 700 °C and milled LNS\_700 powder between 900 °C–1300 °C and b) LAS\_xero and powders obtained by calcination of the LAS\_xero at 600 °C and milled LAS\_600 powder between 900 °C–1300 °C in air; and the lanthanum silicate powders c) LNS\_900 and d) LAS\_900, heat treated at 900 °C, milled for 30 min and subsequently calcined at 1300 °C and 1500 °C. Note that the enlarged part of the patterns between  $2\theta = 25 - 40^\circ$  was shown to get a better insight in the presence of impurities. (Colour online)

kers,<sup>24</sup> demonstrated that  $\text{La}_2\text{SiO}_5$  and  $\text{La}_2\text{Si}_2\text{O}_7$  can react by diffusion, and thus form the apatite phase according to the following reactions ((Eq. (6) and (7)):



A milling step was introduced after the calcination to reduce the particle size and thus the diffusion paths in the LNS\_900 and LAS\_900 powders, and consequently to increase the reactivity. The calcination of the as-milled powder at 1300 °C resulted in a lower amount of impurities (see Fig. 7c, 1300 °C), while the calcination at the elevated temperature of 1500 °C promoted the formation of the pure, well-crystallized  $\text{La}_{9,33}\text{Si}_6\text{O}_{26}$  phase. The crystallite size of the  $\text{La}_{9,33}\text{Si}_6\text{O}_{26}$  powder was calculated from the broadening of the apatite reflections using the Debye-Scherrer equation (Eq. (4)). It was found that the crystallite size of the  $\text{La}_{9,33}\text{Si}_6\text{O}_{26}$  calcined at 1000 °C and 1500 °C is 66.1 nm and 99.7 nm, respectively.

Both LAS\_xero and LAS\_xero heated at 600 °C were XRD-amorphous (see Fig. 7b). Unfortunately, further heating at 900, 1000 °C or 1300 °C did not give rise to the formation of the pure apatite phase. Even after the introduction of an additional milling step and calcination at 1300 °C and 1500 °C (see Fig. 7d) the situation stayed unchanged. Obviously, the fast kinetics of the hydrolysis and condensation reactions of the nitric-acid catalyzed synthesis (see section 3.1) lead to a non-homogeneous gel, and consequently to appearance of a huge amount of impurities in the calcined powder, which could not be easily removed. Therefore this powder was not considered for further study.

The formation of the pure apatite phase from the LNS-xerogel to the crystalline powder was also followed by FTIR spectroscopy. Fig. 8 shows the FTIR spectrum of the LNS-xerogel calcined at various temperatures (700 °C–1300 °C) and LNS\_900, additionally calcined at 1300 °C and 1500 °C. The weak broad bands centered around 1474  $\text{cm}^{-1}$  and 1392  $\text{cm}^{-1}$ , observed in the spectrum of the powder calcined at 700 °C are indicative of organic residuals, as confirmed by disappearance of the corresponding bands in the sample heated at higher temperatures. The band centered at 863  $\text{cm}^{-1}$  could be assigned to symmetric vibrations of the Si-O-Si bonds, belonging to the ring structure of the  $\text{SiO}_4$  tetrahedral network. We observed that at the higher temperatures it becomes sharper.<sup>6,25</sup> A similar situation is observed for the mode located at 989  $\text{cm}^{-1}$ , due to asymmetric stretching vibration of the Si-O-Si bond in isolated  $\text{SiO}_4$  tetrahedra of the apatite.<sup>6,25</sup> The band at 475  $\text{cm}^{-1}$ , observed in the spectrum of the powder calcined at 700 °C, is due to the Si-O-Si bending vibration.<sup>26</sup> This band transforms at higher temperatures to the band with a fine structure. The modes at 538  $\text{cm}^{-1}$ , 500  $\text{cm}^{-1}$ , 458

$\text{cm}^{-1}$  and 376  $\text{cm}^{-1}$  are related to asymmetric and symmetric vibrations in  $\text{SiO}_4$  tetrahedra of apatite.<sup>6</sup> The La-O modes cannot be easily observed, since the Si-O-Si bonds in the measured spectral range (4000–400  $\text{cm}^{-1}$ ) are much stronger than the La-O bonds.<sup>25</sup> According to literature data,<sup>6,25</sup> the bands connected with the presence of secondary phases, could be detected at 374  $\text{cm}^{-1}$  ( $\text{La}_2\text{O}_3$ ,<sup>25</sup>), 795  $\text{cm}^{-1}$ , 623  $\text{cm}^{-1}$  and 484  $\text{cm}^{-1}$  ( $\text{SiO}_2$ ,<sup>25</sup>) or 669  $\text{cm}^{-1}$  ( $\text{La}_2\text{Si}_2\text{O}_7$ ,<sup>6</sup>). To the authors' knowledge there is no literature data linked to the position of the  $\text{La}_2\text{SiO}_5$  bands in the FTIR spectrum of the lanthanum silicate. In the spectrum of the sample obtained after calcination of the LNS\_700 powder at 1300 the weak bands at 641  $\text{cm}^{-1}$  and 1101  $\text{cm}^{-1}$  were found. These bands may be connected with vibration modes of the  $\text{La}_2\text{Si}_2\text{O}_7$  and maybe  $\text{La}_2\text{SiO}_5$  impurities, respectively. The absence of the vibration modes related to impurities in the spectrum of the LNS\_900, milled and subsequently calcined at 1300 °C, could be explained by a small amount of impurities. Other spectra shown in Fig. 8 indicate the phase purity of the as-prepared powders.

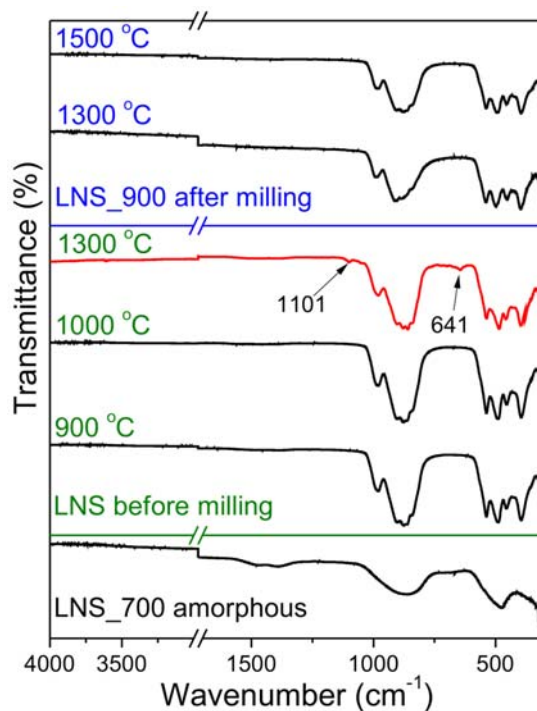


**Figure 8.** FTIR spectra of the  $\text{La}_{9,33}\text{Si}_6\text{O}_{26}$  powders calcined at various temperatures. (Colour online)

Powders calcined at 1000 °C and 1500 °C were analyzed by FE-SEM (Fig. 9). It was difficult to evaluate the particle size, as the powders were agglomerated. In the powder calcined at 1000 °C the particle size is about 100–200 nm. The particle size tends to increase with increasing calcination temperature. After heating at 1500 °C, the particle size is about 500–700 nm.

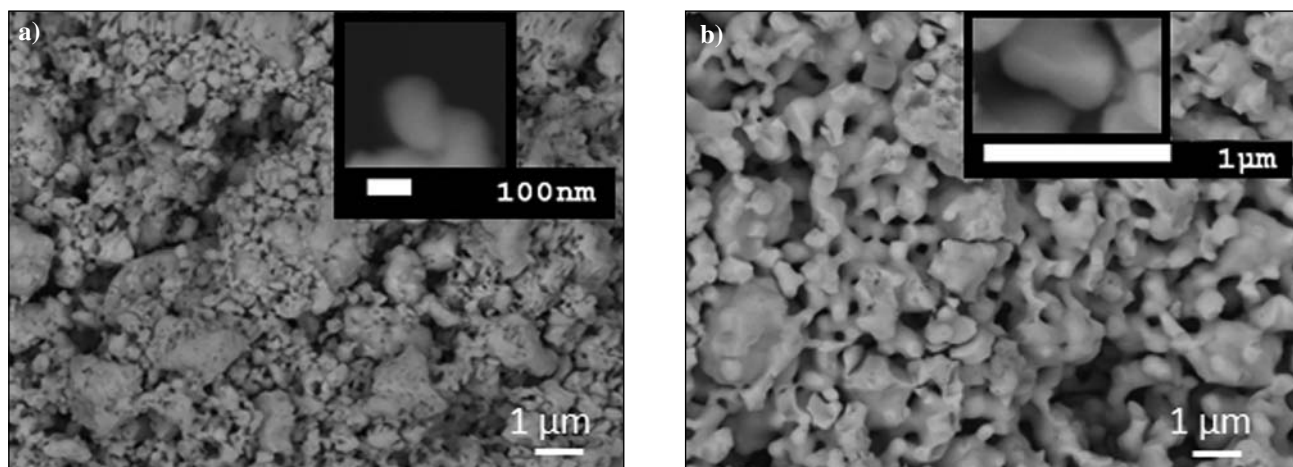


Figure 9. FE-SEM micrographs of phase-pure  $\text{La}_{9.33}\text{Si}_6\text{O}_{26}$  powders calcined at 1000 °C (a) and 1500 °C (b)

### 3. 3. Characterization of Ceramics

The powder calcined at 900 °C was wet milled for 30 min in a planetary mill to break up the agglomerates. The granulometric result, shown in Fig. 10, indicated that the median particle size ( $d_{50}$ ) was 0.6 µm, while 90% of the particles ( $d_{90}$ ) were smaller than 1.6 µm.

The powder compacts with 56% of theoretical density (TD), obtained by cold-isostatic pressing at 400 MPa, were sintered at 1400 °C for 3 h in air with two different heating rates: 5 °C/min and 2 °C/min. The phase composition and microstructure of the sintered samples with 88% and 94% TD, respectively were analysed and the results are collected in Fig. 11. Decreasing the heating/cooling rate from 5 °C/min to 2 °C/min, the period required to achieve the final temperature, as well as the period for the pore elimination was prolonged, thus the higher densities were achieved. According to XRD both ceramic samples are phase-pure  $\text{La}_{9.33}\text{Si}_6\text{O}_{26}$ . The SEM analysis revealed that the bulk of the samples had a dense microstructure with a uniform distribution of porosity.

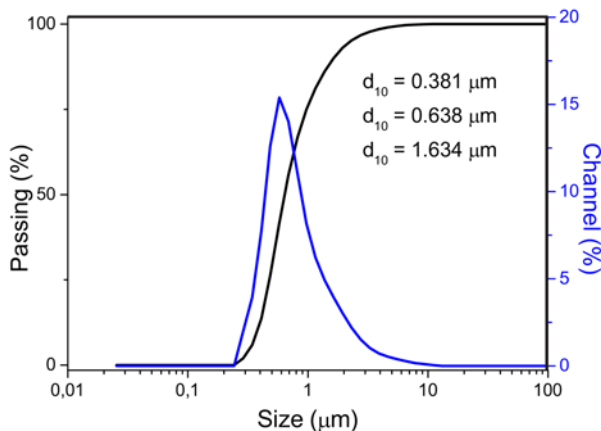


Figure 10. Particle size distribution of the powder calcined at 900 °C and milled for 30 min. (Colour online)

While the small grains and extensive pores are evident from the microstructure of the sample heated with a heating rate of 5 °C/min, the closed porosity is observed in a sample sintered with a low heating rate indicating the final stage of sintering. Thermal etching of the samples allowed to estimate the grain size, which was found to be 0.3–1 µm in the sample sintered with the higher heating rate (5 °C/min) and 0.8–2 µm in the sample sintered with 2 °C/min.

In our work, 94 % dense and single phase  $\text{La}_{9.33}\text{Si}_6\text{O}_{26}$  ceramic was obtained from the phase-pure LNS\_900 powder, synthesised by the sol-gel method, and sintered in air at 1400 °C for 3 h with a heating rate of 2 °C/min. In comparison to the results reported for the sol-gel,<sup>27</sup> and solid-state synthesized,<sup>9–11,28–30</sup>  $\text{La}_{9.33}\text{Si}_6\text{O}_{26}$  ceramic samples, where much higher temperatures, exceeding 1600 °C, and dwell-times longer than 5 h were needed to achieve relative densities close to 85%, in our study both sintering temperature and dwell-time were significantly lowered.

## 4. Conclusion

The synthesis of  $\text{La}_{9.33}\text{Si}_6\text{O}_{26}$  from ethanol solutions of TEOS and lanthanum nitrate with acetic-acid catalyst, or lanthanum acetate with nitric-acid catalyst, in the transition from liquid to amorphous and crystalline states was analysed and discussed. The TG-DTA analysis of the lanthanum salts showed that the amount of water in the nitrate is three times higher than in the acetate. FTIR analysis indicated that lanthanum ions are strongly coordinated to the nitrate ions in both sols. The lanthanum environments were not changed by the addition of TEOS to the LN- or LA-sol. According to the FTIR analysis, the main difference between LNS- and LAS-sols was in the amount of water – a higher amount was found in the latter and related to the azeotropic mixture of the catalyst nitric acid with water.

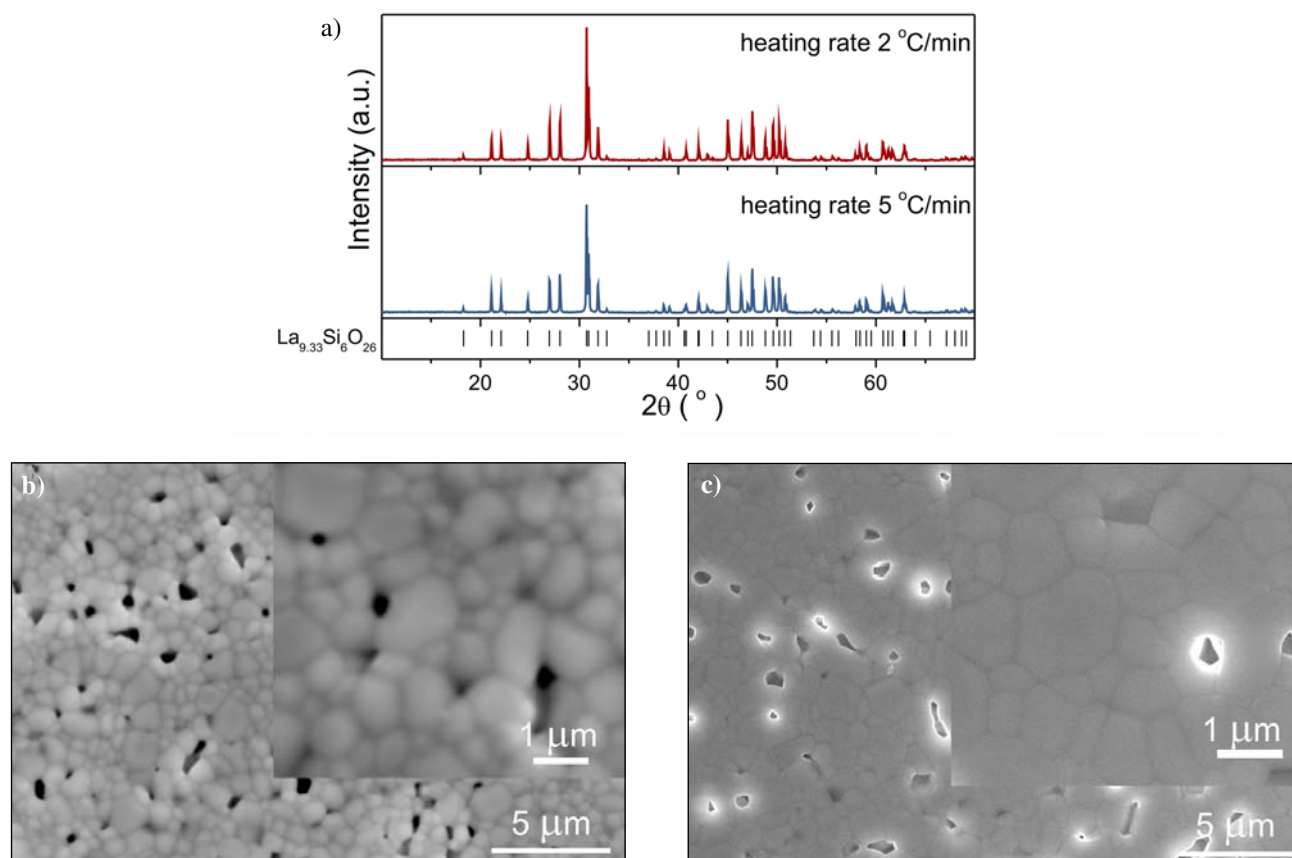


**Figure 11.** XRD patterns a) and SEM micrographs of the  $\text{La}_{9.33}\text{Si}_6\text{O}_{26}$  ceramics sintered to 1400 °C for 3 h with a heating rate of 5 °C/min b) and 2 °C/min c). (Colour online)

Consequently, hydrolysis of the LAS-sol was enhanced, and the gelation time reduced, resulting in a non-homogeneous gel. After calcination of the LAS xerogel powder at 900 °C a huge amount of secondary phases ( $\text{La}_2\text{SiO}_5$  and  $\text{La}_2\text{Si}_2\text{O}_7$ ) beside the matrix  $\text{La}_{9.33}\text{Si}_6\text{O}_{26}$  phase were detected. According to FTIR, a higher amount of water, which promote the siloxane bond hydrolysis, and different bonding of the acetate groups to the La-ligand are listed as a possible reasons for poor homogeneity in the LAS\_gel network and consequently for huge amount of impurities in the powders calcined above 900 °C.

In contrast, the La-nitrate synthesis route with the acetic-acid catalyst ensured a good mixing of the species at the nanometre level resulting in the formation of the pure  $\text{La}_{9.33}\text{Si}_6\text{O}_{26}$  powder at 900 °C. Phase-pure ceramic with 94 % relative density was obtained after sintering at 1400 °C, at about 200 °C lower temperature than usually reported for the apatite material.

## 5. Acknowledgments

This research was financially supported by the Slovenian research agency (research programme P2-0105) and supported by the foundation of the University of Li-

moges. P. Chevreux gratefully acknowledges the welcome of Electronic Ceramics Department at the Jožef Stefan Institute and the collaboration with SPCTS.

## 6. References

1. T. Kharlamova, S. Pavlova, V. Sadykov, T. Krieger, L. Baturev, V. Muzykantov, N. Uvarov, C. Argirusis, *Solid State Ionics* **2009**, *180*, 796–799.
2. L. León-Reina, J. M. Porras-Vázquez, E. R. Losilla, M. A. G. Aranda, *Solid State Ionics* **2006**, *177*, 1307–1315.
3. P. J. Panteix, I. Julien, D. Bernache-Assollant, P. Abélard, *Mater. Chem. Phys.* **2006**, *95*, 313–320.
4. X. J. Chen, K. A. Khor, S. H. Chan, L. G. Yu, *Mater. Sci. Eng. A* **2002**, *335*, 246–252.
5. N. Q. Minh, *J. Am. Ceram. Soc.* **1993**, *76*, 563–798.
6. T. Kharlamova, S. Pavlova, V. Sadykov, M. Chaikina, T. Kreiger, O. Lapina, D. Khabibulin, A. Ischenko, V. Zaikovskii, C. Argirusis, J. Frade, *Eur. J. Inorg. Chem.* **2008**, *2008*, 939–947.
7. S. Nakayama, M. Sakamoto, *J. Eur. Ceram. Soc.* **1998**, *18*, 1413–1418.
8. E. Bechade, I. Julien, T. Iwatab, O. Masson, P. Thomas, E. Champion, K. Fukudab, *J. Eur. Ceram. Soc.* **2008**, *28*, 2717–2724.

9. E. Kendrick, M. Islam Saiful, P. R. Slater, *J. Mater. Chem.* **2007**, *17*, 3104–3111.
10. J. E. H. Sansom, D. Richings, P. R. Slater, *Solid State Ionics* **2001**, *139*, 205–210.
11. J. McFarlane, S. Barth, M. Swaffer, J. E. H. Sansom, P. R. Slater, *Ionics* **2002**, *8*, 149–154.
12. S. Célrier, C. Laberty, F. Ansart, P. Lenormand, P. Stevens; *Ceram. Inter.* **2006**, *32*, 271–276.
13. S. Célrier, C. Laberty-Robert, F. Ansart, C. Calmet, P. Stevens, *J. Eur. Ceram. Soc.* **2005**, *25*, 2665–2668.
14. E. D. Ion, B. Malič, I. Arčon, J. Padežnik Gomilšek, A. Kodre, M. Kosec, *J. Eur. Ceram. Soc.* **2010**, *30*, 569–575.
15. B. Klingenberg, M. A. Vannice, *Chem. Mater.* **1996**, *8*, 2755–2768.
16. S. M. R. Rocha, C. A. S. Queiroz, A. Abrão, *J. Alloys Compd.* **2002**, *344*, 389–393.
17. G. Liptay (Ed.): Atlas of Thermoanalytical Curves, Heyden, London, **1975**, *4*, pp. 229.
18. B. M. Gatehouse, S. E. Livingstone, R. S. Nyholm, *J. Chem. Soc.* **1957**, *0*, 4222–4225.
19. C. J. Brinker, G. W. Scherer, Sol-gel science, **1990**, London: Academic Press.
20. S. Qingle, L. Lihua, Z. Yanwei, Z. Hua, *J. Wuhan Univ. Technol. Mater. Sci. Ed.* **2012**, *27*, 841–846.
21. G. B. Deacon, R. J. Phillips, *Coord. Chem. Rev.* **1980**, *33*, 227–250.
22. L. Predoana, A. Jitianu, B. Malič, M. Zaharescu, *J. Am. Ceram. Soc.* **2012**, *95*, 1068–1076.
23. E. D. Ion, B. Malič, M. Kosec, *J. Eur. Ceram. Soc.* **2007**, *27*, 4349–4352.
24. K. Fukada, T. Asaka, M. Oyabu, D. Urushihara, A. Berghout, E. Bechade, O. Masson, I. Julien, P. Thomas, *Chem. Mater.* **2012**, *24*, 4623–4631.
25. E. Rodriguez-Reyna, A. F. Fuentes, M. Maczka, J. Hanuza, K. Boulahya, U. Amador, *J. Solid State Chem.* **2006**, *179*, 522–531.
26. R. F. S. Lenza, W. L. Vasconcelos, *Mat. Res.* **2001**, *4*, 189–194.
27. H. Yoshioka, *J. Alloys Compd.* **2006**, *408–412*, 649–652.
28. H. Yoshioka, *J. Am. Ceram. Soc.* **2007**, *90*, 3099–3105.
29. A. L. Shaula, V. V. Kharton, F. M. B. Marques, *J. Sol. State Chem.* **2005**, *178*, 2050–2061.
30. S. Tao, J. T.S. Irvine, *Mat. Res. Bull.* **2001**, *36*, 1245–1258.

## Povzetek

V prispevku poročamo o kislinsko katalizirani sintezi  $\text{La}_{9,33}\text{Si}_6\text{O}_{26}$  iz lantanovega nitrata ali acetata in silicijevega etoksida (TEOS) v etanolu med prehodom iz tekoče v amorfno ter kristalinično fazo. Podobnost infrardečih spektrov raztopin lantanovih spojin in lantan-silicijevih solov nakazuje, da ostane lokalna urejenost lantanovih atomov nespremenjena med reakcijo lantanovih reagentov in TEOS. Pri sintezi lantanovega silikata, ki je bila katalizirana z dušikovo kislino, poteče reakcija hidrolize hitro, kar posledično vodi do kemijsko heterogenega produkta. Pri sintezi, ki je katalizirana z očetno kislino, dosežemo dobro mešanje reagentov na nanometriškem nivoju in s segrevanjem prekursorja pri 900 °C pripravimo enofazni prah  $\text{La}_{9,33}\text{Si}_6\text{O}_{26}$ . Enofazno keramiko z relativno gostoto 94 % smo pripravili s sintranjem pri 1400 °C 3 ure na zraku, kar je 200 °C nižje od običajnih temperatur sintranja tega apatitnega materiala.